



Tungsten-Based Polyoxometalate-Ionic Liquid as Lubricant Additive for Low-Viscosity PAO: Effect of Steel Composition and Microstructure on the Boundary Lubricating Performance

M. L. Casasin-Garcia¹ · S. G. Mitchell² · N. Espallargas¹

Received: 21 March 2025 / Accepted: 18 June 2025
© The Author(s) 2025

Abstract

The development of environmentally acceptable lubricants and lubricant additives has become a focal point within tribology due to increasing regulatory and sustainability demands. In this context, low-viscosity lubricants are gaining attention for their potential to reduce energy losses. However, their performance under a boundary lubrication regime, where thinner oil film build-up is present, requires more efficient boundary additives. This work evaluates a polyoxometalate-ionic liquid (POM-IL) as a multifunctional boundary additive in a low-viscosity polyalphaolefin-based lubricant, comparing its performance to zinc dialkyldithiophosphate (ZDDP) and a halogen-containing ionic liquid (IL). Tribological tests on AISI 316L stainless steel and AISI 52100 bearing steel revealed that while ZDDP showed substrate-independent adsorption and tribological performance, the IL-based additives had substrate-dependent behaviour. Strong chemisorption was consistent for both IL-based additives, yet their anti-wear and friction-reducing properties differed, showing evidence for the presence of a combined mechanism that includes both strong adsorption and tribochemical reactions. Additionally, the interaction between POM-ILs' negatively charged surfaces, W atoms, and Cr(III) in 316L was identified as a key factor in their performance. Notably, significant work-hardening was observed in 316L lubricated with POM-IL-containing blends, further enhancing its anti-wear properties. These findings emphasize the role of substrate chemistry in boundary lubricant additive performance in low-viscosity lubricants, offering insights for the development of more efficient multifunctional boundary lubrication solutions.

Keywords POM-IL · Boundary lubrication · Environmentally acceptable lubricants · Green tribology

1 Introduction

Lubricants are essential for the optimal functioning of mechanical systems and machinery, acting as crucial components in their tribological systems. Mechanical systems require efficient lubrication to control friction, and limit wear and heat between the contacting surfaces. The lubricant's physical and chemical requirements vary significantly

depending on the specific system of interest. In hydrodynamic lubrication, a continuous lubricant film separates both surfaces, preventing contact, and minimizing friction and wear. On the other hand, boundary lubrication relies on the friction-reducing and anti-wear properties of the lubricant additives, as physical contact between the surfaces is unavoidable. Consequently, the formulation of lubricants is tailored to the lubrication regime of the application. Recent incentives by governing agencies and institutions to promote environmentally conscious alternatives in various technical fields have significantly impacted efforts towards lubricating strategies [1]. There is considerable motivation to develop both, energy efficient and environmentally acceptable lubricants and additives. One of the strategies to develop more energy efficient base lubricants is the shift towards low-viscosity fluids, due to their potential to reduce energy losses. However, their performance under a boundary lubrication

✉ N. Espallargas
nuria.espallargas@ntnu.no

¹ Department of Mechanical and Industrial Engineering, Norwegian Tribology Center, Norwegian University of Science and Technology (NTNU), Trondheim, Norway

² Instituto de Nanociencia y Materiales de Aragón (INMA-CSIC/UNIZAR), Consejo Superior de Investigaciones Científicas, Universidad de Zaragoza, Saragossa, Spain

regime, where thinner oil film build-up is present, requires more efficient boundary additives.

The functionality of a lubricant primarily arises from the chemical additives within the blend, typically constituting 1–30% of the formulated lubricant, with the remaining being base lubricant(s). Each desired function, such as friction reduction, anti-wear, antioxidation or corrosion inhibition, is achieved through specific chemical additives. Generally, the more functionalities a lubricant requires, the greater the number of additives needed in the blend. This can lead to drawbacks, including competition among surface-active components for adsorption sites [2], antagonistic effects between different chemical species [3], and increased formulation complexity.

In the boundary lubrication regime, where high loads and low speeds are present, anti-wear and extreme pressure (EP) additives are particularly useful. EP additives are generally organic compounds that contain P, S, or Cl atoms within their structure [4], while some of the most common anti-wear additives are zinc dialkyldithiophosphates (ZDDPs), a family of compounds containing Zn, S, and P atoms in their structures [5]. Although ZDDP forms protective films on metallic surfaces under tribological conditions, it undergoes thermal decomposition processes that produce ashes that are detrimental to the environment [6]. In addition, ZDDPs are harmful or toxic to aquatic life and are not readily biodegradable, with long-lasting consequences to the environment [7].

Classical lubricant additives have seen a growing competition from new materials with promising properties. Ionic liquids (ILs) belonging to this category have been a focus for tribologists since the early 2000s [8]. The fast success of ILs in tribology arises from their compelling properties including low volatility and melting point, non-flammability, and high thermal stability [8–10]. The family of ILs is large and many of the structures that have been studied, although performing well for tribology, contain halogen atoms, which render the additive, and thus the lubricant, non-compliant with environmental demands, that is indeed the case for one of the additives used for comparison in this work.

In response to the growing environmental demands, this study has chosen a new class of materials, polyoxometalate-ionic liquids (POM-ILs), for their potential multifunctionality as lubricant additives and their documented greener chemistry compared to more traditional additives [11–13]. Although assessing the overall toxicity of ILs and POM-ILs remains challenging, the removal of halogen anions, aromatic cations, and particularly imidazolium-based cations represents a meaningful step towards more sustainable lubricant additive design.

In a previous study, POM-ILs have shown to be effective lubricant additives in different base fluids when tested on AISI 316L stainless steel [14]. In the present work, the best POM-IL in a low-viscosity polyalphaolefin

(PAO) from the previous study has been chosen for a detailed friction and wear study in boundary lubricating conditions. A Keggin undecatungstosilicate ($\text{SiW}_{11}\text{O}_{39}^{8-}$) polyoxometalate (POM), combined with ammonium cations to form the POM-IL, has been tested and compared with ZDDP and a pyrrolidinium fluorine-based IL on different metal substrates. Since the boundary lubricating conditions are crucial for low-viscosity lubricants, the metal substrate is key in the understanding of the additive performance. Therefore, this work aims to investigate how the metal substrate's composition and microstructural parameters influence its interaction with the additives. Consequently, AISI 52100 bearing steel and AISI 316L have been chosen for comparison due to their different composition and microstructure. The applications of these metal substrates are distinct, and their performance in tribological settings varies. Both materials, however, would benefit from tailored lubricant packages to achieve optimal efficiency under any rubbing conditions. Friction and wear tests were conducted and supported by adsorption studies with iron and stainless steel-coated quartz sensors. The worn discs were thoroughly characterized using X-ray photoelectron spectroscopy (XPS) and scanning electron microscopy with a focussed ion beam (SEM-FIB).

2 Experimental

2.1 Materials

2.1.1 Additives and Base Fluid

In this work, the following chemical species were used as lubricant additives: a POM-IL formed from a silicotungstate Keggin polyoxometalate and trihexyltetradecylammonium cations, $[\text{SiW}_{11}\text{O}_{39}][\text{THTDA}]_8$, abbreviated as $\text{SiW}_{11}\text{THTDA}$, synthesised as described in the literature [15, 16]; a pyrrolidinium-based IL, 1-butyl-1-methylpyrrolidinium tris(pentafluoroethyl) trifluorophosphate (BMP), purchased from Sigma Aldrich; and a well-known anti-wear additive, Zinc dialkyldithiophosphate (ZDDP), purchased from Lanxess. Table 1 shows the chemical structure, name, and abbreviation of these species.

The base lubricant for these additives was a low-viscosity (8 cSt at 100 °C) polyalphaolefin (PAO8) provided by Chevron Phillips. The hydrocarbon structure of PAO8 is a mixture resulting from the oligomerization of linear α -olefins with a variable number of C atoms in the chain. The formulated lubricants contained 1 wt.% of each additive. This concentration has been chosen after testing different blend concentrations, where 1 wt.% showed the most consistent results.

Table 1 Compounds used as lubricant additives in this work

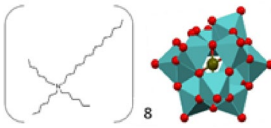
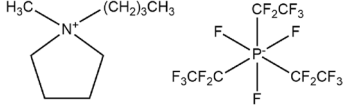
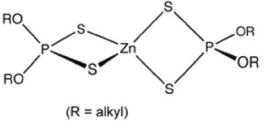
Additive			
Name	[Trihexyltetradecyl-ammonium] ₈ [SiW ₁₁ O ₃₉]	1-Butyl-1-methylpyrrolidinium tris(pentafluoroethyl) trifluorophosphate	Primary zinc dialkyldithiophosphate
Abbreviation	SiW ₁₁ THTDA	BMP	ZDDP

Table 2 Chemical composition, microstructure, and hardness of the metal substrates

Composition	316L	52,100
C	< 0.03%	0.98 – 1.10%
Cr	16.5 – 18.5%	1.3 – 1.6%
Ni	10 – 14%	-
Mo	2 – 3%	-
Mn	≤ 2%	0.25 – 0.45%
Si	≤ 1%	0.15 – 0.35%
P	≤ 0.045%	≤ 0.025%
S	≤ 0.03%	≤ 0.025%
Microstructure	Austenitic	Ferritic
Vickers hardness	267.9 ± 13.3	± 4.5

The blending process of the additives and the base lubricant consisted of magnetic stirring for 6 h at 60 °C followed by a 30 min ultrasonic bath (VWR USC300T model with a frequency of 35 kHz and power of 180 W). Then, the lubricant blends were visually assessed to ensure optimal miscibility before testing. While ZDDP formed a well-dissolved mixture, both BMP and SiW₁₁THTDA formed emulsions (Figure S1) and were considered stable enough for the purposes of the study as no fast phase separation was observed.

2.1.2 Metallic Substrates

Two substrates that differ in their chemical composition, microstructure, and mechanical properties have been chosen for this work (Table 2). AISI 52100 (52,100) and AISI 316L (316L) steels stand apart in their chemical composition and the heat treatments they undergo during processing. This results in different microstructures that translate into higher wear resistance for 52,100, while 316L, enriched with chromium, nickel, and molybdenum, excels in corrosion resistance. While 316L primarily presents an austenitic microstructure (with equiaxial grains), 52,100 consists of a ferritic structure with a homogeneous distribution of chromium-rich iron carbides, as can be observed from Fig. 1

The former is a face-centred cubic (FCC) crystal structure stabilized by the presence of nickel [17], whereas the latter can undergo different heat treatments to achieve different microstructures and thus hardness, i.e. from very low hardness after an annealing process to high hardness after a quenching process. In this work, the annealed version of the 52,100 steel has been chosen to rule out the effect of hardness on the wear performance. Thus, the composition and microstructure of the steels remain as the main parameters of study.

2.2 Tribological Testing Parameters

The tribological testing consisted of a reciprocal ball on disc test, with 52,100 and 316L discs and alumina ball. The metal samples were cut in the form of cylindrical discs of 3 cm diameter and 6 mm thickness, and, before testing, they were surface prepared by polishing plates according to Struers manufacturer guidance [18] until the desired roughness of around $Ra = 0.090 \pm 0.003 \mu\text{m}$ was achieved. Once polishing was completed, an ultrasonic bath cleaning process in ethanol (and water for 316L) was performed for 5 min to remove any potential residues from the polishing steps. The tribological testing was performed in a tribometer (Tribocorr Resmat Corporation, Canada) consisting of rubbing the steel samples alongside 1 mL of the prepared lubricant blend against a 6 mm diameter Al₂O₃ ball (Precision Ball and Gauge Co., Ltd). The applied normal load was 20 N corresponding to a maximum initial Hertzian contact pressure of 2.05 GPa. The sliding distance was 10 mm at a sliding frequency of 1 Hz, corresponding to a 0.02 m/s linear velocity. The duration of the tests was 5000 cycles (20 mm/cycle), corresponding to a total distance of 100 m. The calculated lambda value according to Hamrock-Dawson Eq. ¹⁹ gives values in the range of 10^{-2} for all tests, thus corresponding to a boundary lubrication regime for all cases. All the tests were performed at room temperature and repeated at least twice to verify the reproducibility of the results. Additional repetitions were performed in case of discrepancies, but in this paper, only the results of two repetitions are shown for simplicity.

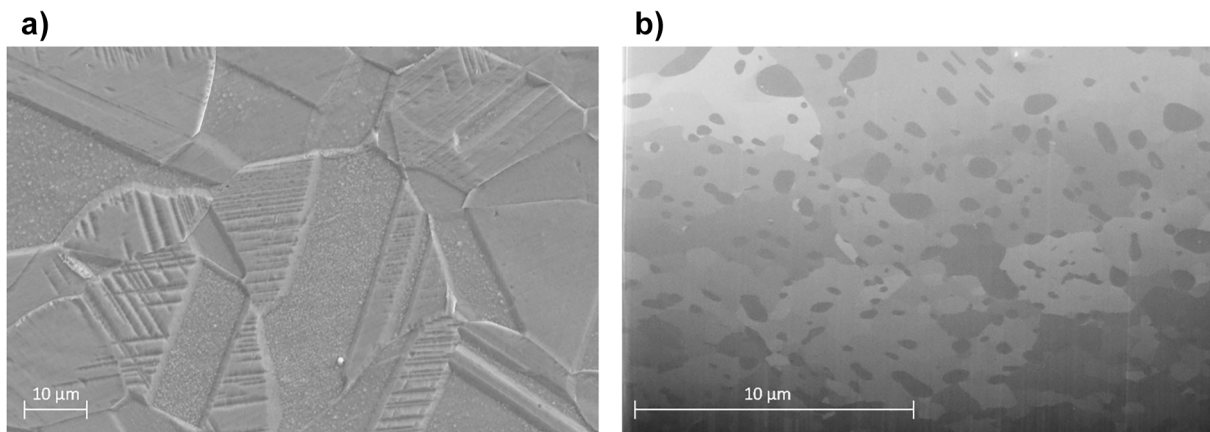


Fig. 1 316L (a) and 52,100 (b) microstructures taken with a scanning electron microscope at different magnifications to showcase the differences in microstructure features

2.3 Surface Adsorption Studies

Additive adsorption studies were run in a quartz crystal microbalance with dissipation mode (QCM-D) from Biolin Scientific. The lubricants containing additives as well as the plain lubricant (PAO8) were tested on stainless steel- and Fe-coated sensors, purchased from RenLux Crystal. The sensors were thoroughly cleaned with ultrasonication and UV-ozone, and then set-up in the instrument to initiate the experiments. A plain base lubricant solution was run through the tubing system at a flow of 50 $\mu\text{L}/\text{min}$ until a stabilization of around 20 min was achieved.

Some experiments did not reach optimal quality due to the viscosity of PAO8, which is very high for the QCM-D system. Specifically, the QCM-D measurement of $\text{SiW}_{11}\text{THTDA}$ at 1 wt.% concentration resulted in a very large frequency drop, which interfered with the acquisition of the complete experimental data. To address this, $\text{SiW}_{11}\text{THTDA}$ concentration was decreased for the QCM-D measurements, which allowed satisfactory data collection. This adjustment was necessary to achieve adsorption results for this lubricant blend.

2.4 Materials Characterization

After the tribological testing and before their characterization, the metallic discs were cleaned to remove potential residues or loose particles. The cleaning process involved rinsing with ethanol, followed by submersion in ethanol, while exposed to an ultrasonic bath for approximately 5 min.

2.4.1 Infinite Focus Microscopy (IFM)

The wear was measured using a 3D Alicona infinite focus microscope followed by analysis with MountainsMap

software. Infinite focus microscopy is a technique that allows to capture images with a large depth of field in a single exposure. The image collection was done at three different locations of the wear track. The images are later processed and combined to create a composite 3D image of the whole wear track area allowing to calculate the volumetric material loss. This is later converted into wear parameters for each sample to compare the different tests. The wear parameters used in this paper are the beta value (β) and the specific wear rate (SWR). The respective formulas are [20, 21] as follows:

$$\beta = \frac{A_{\text{groove}} - A_{\text{ridges}}}{A_{\text{groove}}} \cdot 100 \quad (1)$$

$$\text{SWR} = \frac{\text{Wearvolume}}{\text{Normalload} \cdot \text{Slidingdistance}} \quad (2)$$

2.4.2 Scanning Electron Microscopy (SEM)

For assessing the extent of wear on the discs as well as corroborating the information obtained by IFM, FEI Quanta 650 FEG scanning electron microscope (SEM) using an Everhart–Thornley detector (ETD) was used. The wear track of each repetition was imaged at different magnifications. The images were used to compare the different blends through the visual inspection of top view appearance as well as wear track width. Only one image per sample is shown for simplicity, but all repetitions revealed the same characteristics.

2.4.3 Scanning Electron Microscope and Focussed Ion Beam (SEM–FIB)

A dual beam SEM with a focussed ion beam (FEI Helios G4 UX Nanolab DualBeam) equipped with an in-chamber secondary electron detector (ICE) was used to prepare and

study the wear track cross-sections of the metal substrates. The cross-section images were taken at the centre of the wear scar, both length and width, and perpendicular to the sliding direction. A strong protection layer necessary for the subsequent milling of the material to generate the cross-sections at around 35 μm depth was obtained with electron-carbon deposition (5 kV, 13 nA) followed by ion-carbon deposition (30 kV, 0.26 nA). These cross-sections provided insight into the extent of deformation, the presence of tribofilm and grain morphologies, of both deformed and bulk material.

2.4.4 Scanning Transmission Electron Microscopy (STEM)

After carrying out the protection of the surface and milling steps to achieve the cross-section images, a thin (less than 60 nm) lamella was prepared for SiW₁₁THTDA on 316L. The process started by carrying out a J-cut on the cross-section, followed by extracting the lamella with the manipulator. Once achieved, the lamella was mounted on a copper TEM grid, thinned, and cleaned until electron transparency was achieved. The lamella was then studied with scanning transmission electron microscopy (STEM) in a Helios G5 plasma focussed ion beam using a retractable STEM detector with a voltage of 30 kV and current of 0.2 nA.

2.4.5 X-ray Photoelectron Spectroscopy (XPS)

XPS analysis was carried out on both types of metallic discs using a Kratos AXIS Supra spectrometer equipped with a monochromatic Al_{K α} X-ray source 120 W (8 mA/15 kV). A pass energy of 20 eV was utilized, and the analysis comprised an area of 700 \times 300 μm . All analysed binding energies were calibrated by reference of the C 1 s peak at 284.6 eV.

For each metal, XPS analysis was carried out both inside and outside of the wear track. The initial step involved a survey scan, which provided a broader overview by sweeping across a wide range of binding energies to identify elements present on the metal surfaces. This was followed by high-resolution scans, which focussed on narrower binding energy windows corresponding to specific elemental regions, used for detailed chemical analysis. Table 3 summarizes the binding energy ranges used for these high-resolution scans. All data were analysed using the CasaXPS software.

2.4.6 Vickers Hardness Measurements

The hardness of selected samples was measured using a HM-200 series micro-Vickers hardness tester, applying 0.5 N of indentation force. The average of at least 10 indents is taken for reporting the hardness Vickers number (HVN) values alongside the standard deviation.

Table 3 Binding energy regions studied during XPS analysis and corresponding elements

Additive	Element(s)	Binding energy region (eV) [22]
SiW ₁₁ THTDA	W	27–42
BMP	P, F	675–700
ZDDP	S, P, Zn	125–180

3 Results

3.1 Friction Results

Figure 2a shows a long (~40 m) running-in period with high coefficient of friction (CoF) for PAO 8. The additives in PAO8 showed all shorter running-in periods for 316L. The duration of the running-in differed between the additives. Notably, ZDDP had the shortest running-in period, while BMP and SiW₁₁THTDA had a more similar behaviour. Overall, after the running-in period, all additives decreased the average CoF by 50% compared to plain PAO8.

In the case of 52,100, no running-in was observed. Plain PAO8 had the highest average CoF, and ZDDP and BMP the lowest. SiW₁₁THTDA was halfway between the two. Additionally, BMP showed a sharp increase in friction towards the end of the test (at around 80 m distance), getting closer to the CoF of the POM-IL.

3.2 Wear Characterization—IFM

Figure 3a shows that plain PAO8 resulted in the highest wear rate in 316L, whereas all additives significantly reduced the wear rate. The beta (β) values for 316L are around 40% for both IL-based additives (BMP and SiW₁₁THTDA), indicating that the material loss was primarily driven by plastic deformation. In contrast, the beta value increased to 60% for ZDDP and 70% for plain PAO8, indicating a higher contribution of abrasive wear in these cases.

Contrarily, Fig. 3b shows that the wear rate of plain PAO8 was similar to that of the additive-containing blends in 52,100, with the exception of ZDDP, which showed a significant reduction in wear. The β values for this substrate showed a different behaviour compared to 316L. Both BMP and SiW₁₁THTDA exhibited higher beta values, around 60%, suggesting that abrasive wear and plastic deformation were present. The plain base lubricant showed a beta of around 50%, while ZDDP had the lowest β value (20%), indicating that plastic deformation surpassed over abrasive wear in this case. Interestingly, the wear rate achieved by the additive-containing PAO8 in 316L showed a similar range as for 52,100, already hinting at a potential strengthening effect of the additives.

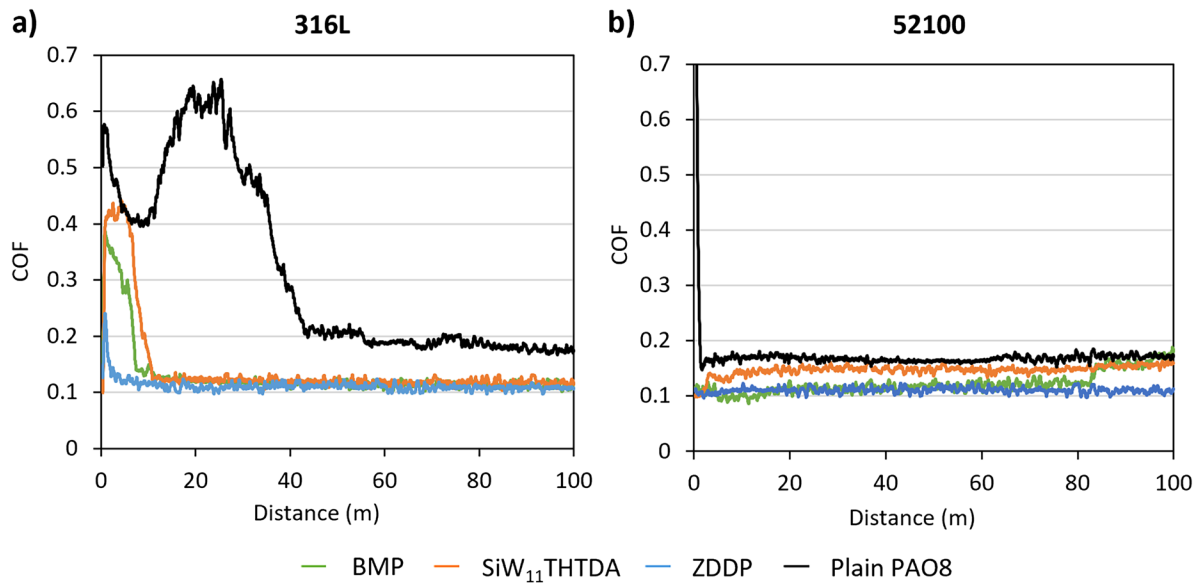


Fig. 2 Friction evolution of the different lubricant blends in both 316L (a) and 52,100 (b). The second repetition of the friction evolution is shown in Figure S2 of the supplementary material. Part of this dataset has been previously reported in another publication [14].

A series of shorter duration tests, with similar conditions, were carried out to study the friction and wear during only the initial running-in period for 316L. The friction data for this set of experiments are found in Figure S3 in the supplementary material

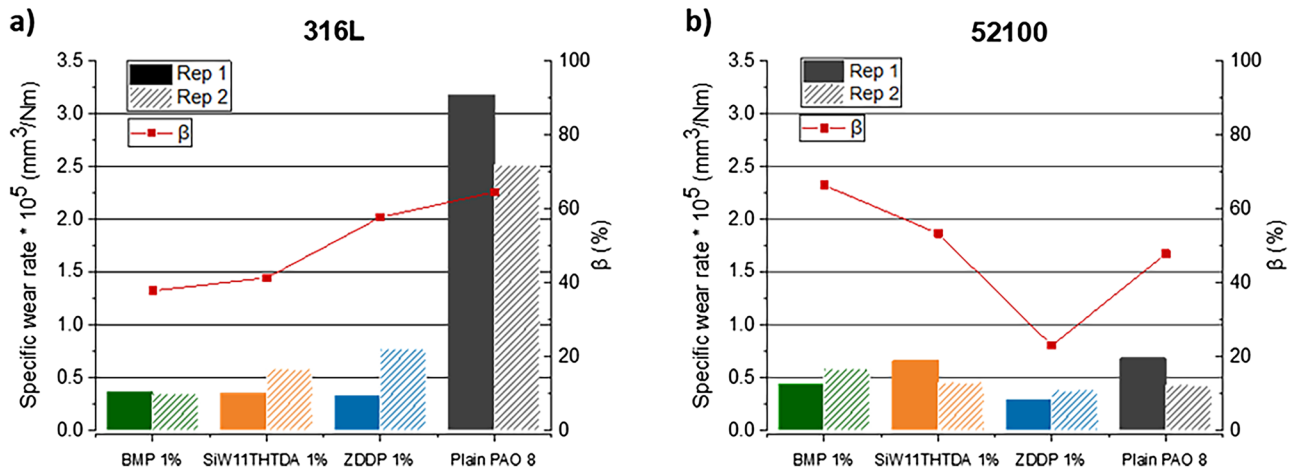


Fig. 3 Measured SWR and β values for the different lubricants in 316L (a) and 52,100 (b) substrates. Part of this dataset has been previously reported in a different publication [14]. A series of shorter duration tests, with similar conditions, were carried out to study the

friction and wear during only the initial running-in period for 316L. The SWR data for this set of experiments are found in Figure S4 in the supplementary material

3.3 Wear Characterization—SEM

Figure 4 illustrates the top view morphologies of the wear tracks of the two metallic substrates tested with the different lubricants.

The abrasive wear was more significant for 316L than 52,100, as a consequence of their different wear resistance, as can be clearly observed for plain PAO8 in both metals.

Within 316L, all additives had a clear effect on the extent of abrasion compared to plain PAO8. BMP showed different

regions inside the wear track, where a smoother section in the middle of the wear track is surrounded by regions of higher abrasion and delamination. SiW₁₁THTDA, on the contrary, showed a homogeneous smoothing of the wear track, with a small number of abrasive grooves present throughout. A similar effect can be observed for ZDDP, where a significant decrease in abrasion is clear.

52,100, as was expected from the wear data, shows generally a significantly smoother wear track morphology. The most notable exception to this is BMP, that similarly to

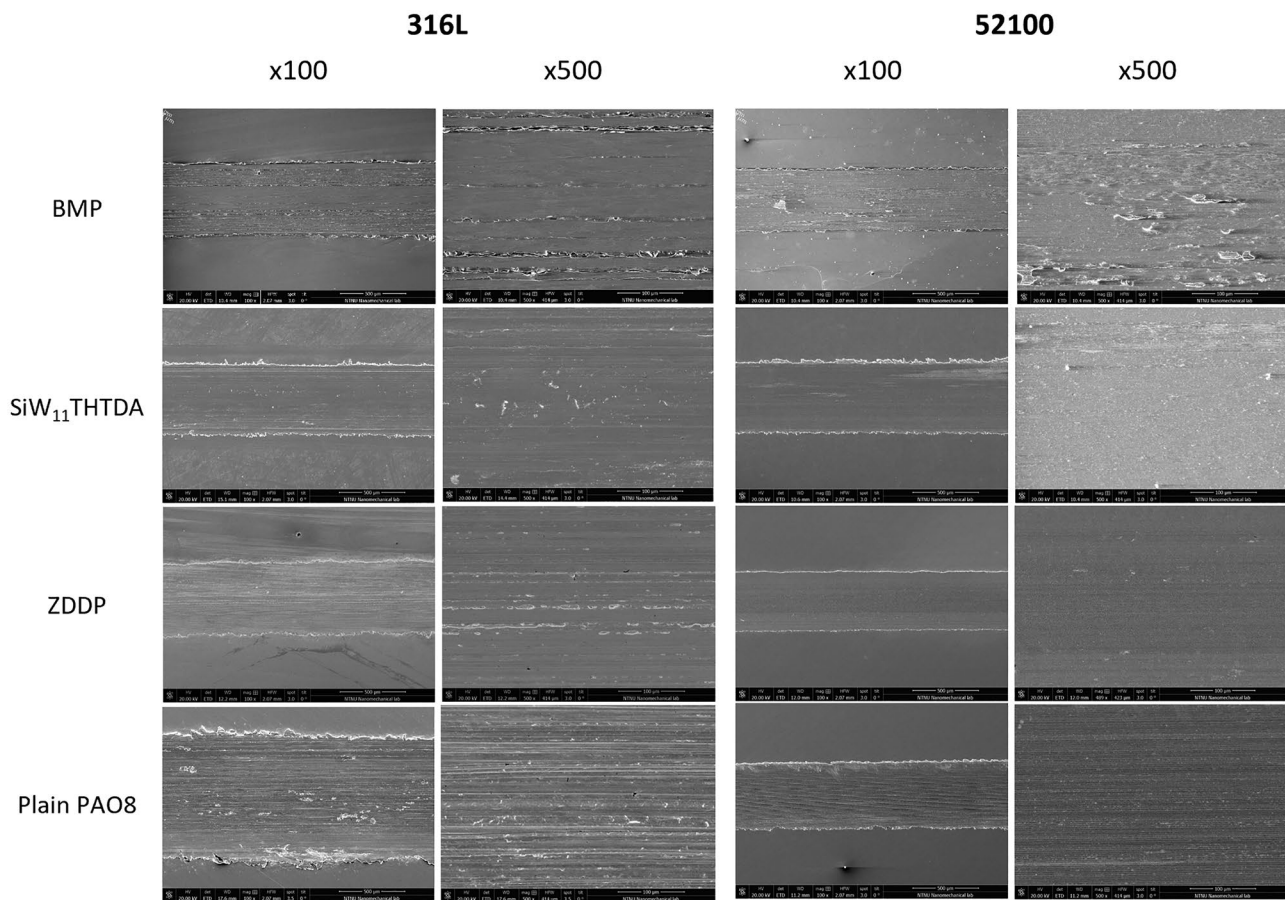


Fig. 4. SEM images at 100 and 500 magnification of wear tracks after tribological testing of all lubricants

316L, shows evidence of material redeposition and delamination in some areas throughout the wear track. The remaining blends and plain PAO8 all show a very similar homogeneously smooth wear track.

3.4 Wear Characterization—SEM–FIB Cross-section

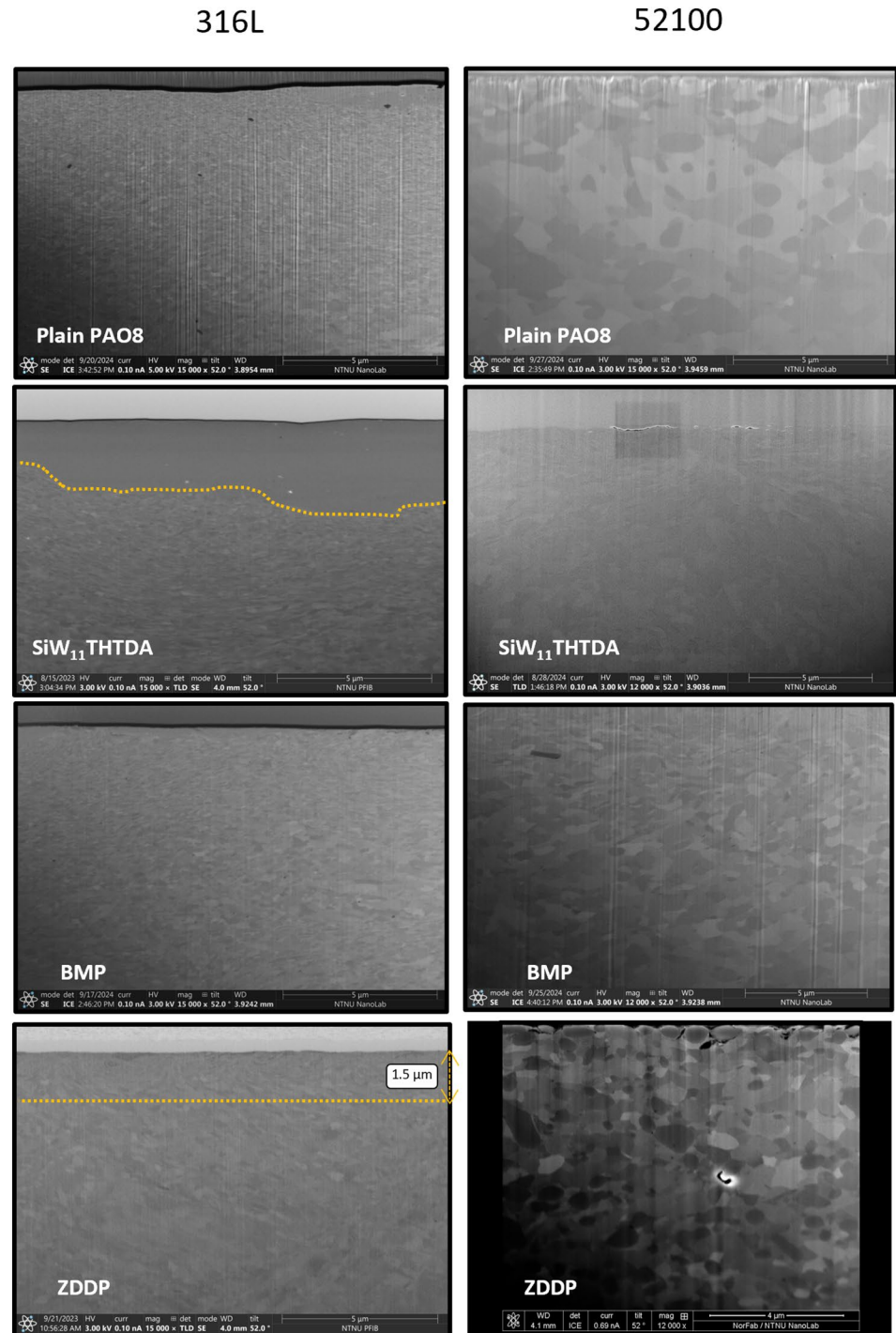
Figure 5 presents the cross-sectional SEM–FIB images of all tested samples. The additives studied in this work exhibit a significant effect on the cross-sectional microstructure of the tested substrates, with notable differences compared to the plain PAO8, especially for 316L.

The cross-section of 316L tested with ZDDP shows minor grain refinement close to the surface, with the bulk structure reappearing at depths beyond approximately 1.5 μm . Additionally, the heterogeneous, darker regions observed at the surface suggest the formation of a patchy tribofilm, in accordance with literature [5]. In contrast, SiW₁₁THTDA shows a distinct region of extreme plastic deformation, approximately 3 μm thick, where significant grain refinement occurs. Beyond this region, plastic

deformation is also observed, however, at a lower extent. BMP displays a large region of plastic deformation with a consistent grain structure throughout the depth. However, the extent of grain size reduction in BMP is less pronounced than in SiW₁₁THTDA. Plain PAO8 exhibits similar behaviour to BMP, with extensive plastic deformation penetrating deeply into the sample. However, plain PAO8 also presents a small region of grain size reduction near the surface, comparable to SiW₁₁THTDA.

All cross-sectional SEM–FIB images of 52,100 show similar morphologies. In addition, all images contain dark circular features corresponding to chromium carbide grains which are particularly visible, especially in the PAO8-ZDDP lubricated sample. Overall, these cross-sections show only minor recrystallization and plastic deformation compared to those of 316L. However, some degree of plastic deformation is visible in the BMP and SiW₁₁THTDA-lubricated samples, appearing as elongated grains closer to the surface. This grain elongation effect is practically absent in the ZDDP and plain PAO8.

Fig. 5 SEM–FIB cross-sectional images of the tested samples on both 316L and 52,100. A yellow dashed line illustrates the differences in microstructure



3.5 Surface Analysis by X-ray Photoelectron Spectroscopy (XPS)

X-ray photoelectron spectroscopy (XPS) analysis was performed to gain insight into the chemical composition of the outer surface of the tested metallic discs. Using CasaXPS software, the survey scan data revealed a relative tungsten (W) concentration of 0.18 at. % inside the wear track of

316L. In contrast, no quantifiable W was detected outside the wear track in 316L, nor in any region of 52,100 (Table 4).

3.6 Additive Adsorption Results

The motivation for carrying out QCM-D measurements was to understand the adsorption behaviour of the different additives on the two metals under study. Figure 6 shows the

Table 4 Elemental quantification of different atoms through survey scan in XPS analysis

% At	316L			52,100		
	SiW ₁₁ THTDA	ZDDP	BMP	SiW ₁₁ THTDA	ZDDP	BMP
W	0.18 (–)	– (–)	– (–)	– (–)	– (–)	– (–)
Zn	– (–)	0.80 (0.35)	– (–)	– (–)	1.36 (0.32)	– (–)
S	– (–)	3.47 (1.3)	– (–)	– (–)	6.05 (–)	– (–)
P	– (–)	– (–)	– (–)	– (–)	6.16 (–)	– (–)
F	– (–)	– (–)	– (–)	– (–)	– (–)	0.40 (–)

The values inside and outside the wear track are represented as *inside (outside)*, a hyphen represents non-detection of that element

frequency (Δf) and dissipation (ΔD) evolution over time. The transitions between fluids are generally accompanied by shifts in both Δf and ΔD . It is important to note that the base lubricant used in these tests exceeded the recommended viscosity for the instrument, leading to some suboptimal data quality. However, trends and differences remain visible, offering valuable insights.

SiW₁₁THTDA was analysed at a concentration of 0.01 wt.% on the 316L substrate, where a significant frequency drop occurred after introducing the additive, suggesting a strong affinity for this substrate. Following rinsing with the plain base lubricant, the frequency remained lower than initial values, likely indicating chemisorption of SiW₁₁THTDA on 316L. This same additive was then studied at a concentration of 0.1 wt.% on 52,100, and similarly to the results on 316L, a significant frequency drop was observed with the addition of the POM-IL. Then, upon rinsing with the plain base lubricant, the frequency remained at lower values than initially, suggesting a strong adsorption on this metal substrate also. ZDDP showed very similar adsorption behaviour on both substrates: approximately three minutes after introducing the additive, a slight frequency drop and dissipation rise occurred, which stabilized quickly. Then, rinsing with plain base lubricant restored both frequency and dissipation to initial values, strongly indicating reversible physisorption in both substrates.

The behaviour of BMP was similar to SiW₁₁THTDA and consistent in both metallic substrates. Upon introduction, BMP caused a sharp decrease in frequency and an increase in dissipation, both of which remained unchanged after reintroducing the plain base lubricant. This suggests strong chemisorption on both metals.

4 Discussion

4.1 Effect of Additive Adsorption on Friction

From the adsorption results, all additives exhibited consistent behaviour, where similar changes in frequency and dissipation were observed, regardless of the substrate (Fig. 6).

However, ZDDP behaved differently from the IL-based additives, showing smaller frequency and dissipation changes. This suggests that ZDDP, absent of a net charge, formed a more rigid and less massive adsorption layer, which desorbed more easily, indicating weaker adsorption. In contrast, both ILs (SiW₁₁THTDA and BMP) showed larger frequency drops (that did not recover) and dissipation changes, suggesting the formation of thicker, softer, and more viscoelastic layers that were strongly adsorbed. It has already been described in the literature [23, 24] that the ionic nature and strong dipole moment of ILs induce high surface affinity, which enhances their interaction with the polarized metal surfaces, where they tend to form a single- or multilayer assembly.

When studying adsorption behaviour, it is important to consider the linear relationship between the resonant frequency change and the adsorbed mass, demonstrated by Sauerbrey in 1959 [25]. According to this relationship (Eq. 3), the change in adsorbed mass (Δm) is proportional to the change in resonant frequency (Δf), where f_0 is the fundamental frequency of the quartz crystal under vacuum, ρ_q is the quartz density, and A accounts for the available crystal surface area. While this model is crucial for understanding frequency changes, it does not account for viscoelastic effects of the adsorbed layer. Nonetheless, the adsorption measurements in this study were performed on a QCM-D, which does account for these viscoelastic effects.

$$\Delta f = -\frac{2f_0^2}{A\rho_q} \Delta m \quad (3)$$

This technique distinguishes between rigid, evenly distributed adsorbed films and softer, viscoelastic adsorbed layers. A rigid film would result in a frequency drop with minimal dissipation increase, while a soft, viscoelastic adsorbed layer would exhibit both, a more significant frequency drop and, especially, dissipation increase, offering understanding into the viscoelastic properties of the adsorbed layers, particularly relevant for liquids and ionic liquids [26].

In theory, a more rigid adsorbed layer, like that formed by ZDDP, would be expected to lead to higher friction due

Stainless steel coated sensor

Fe coated sensor

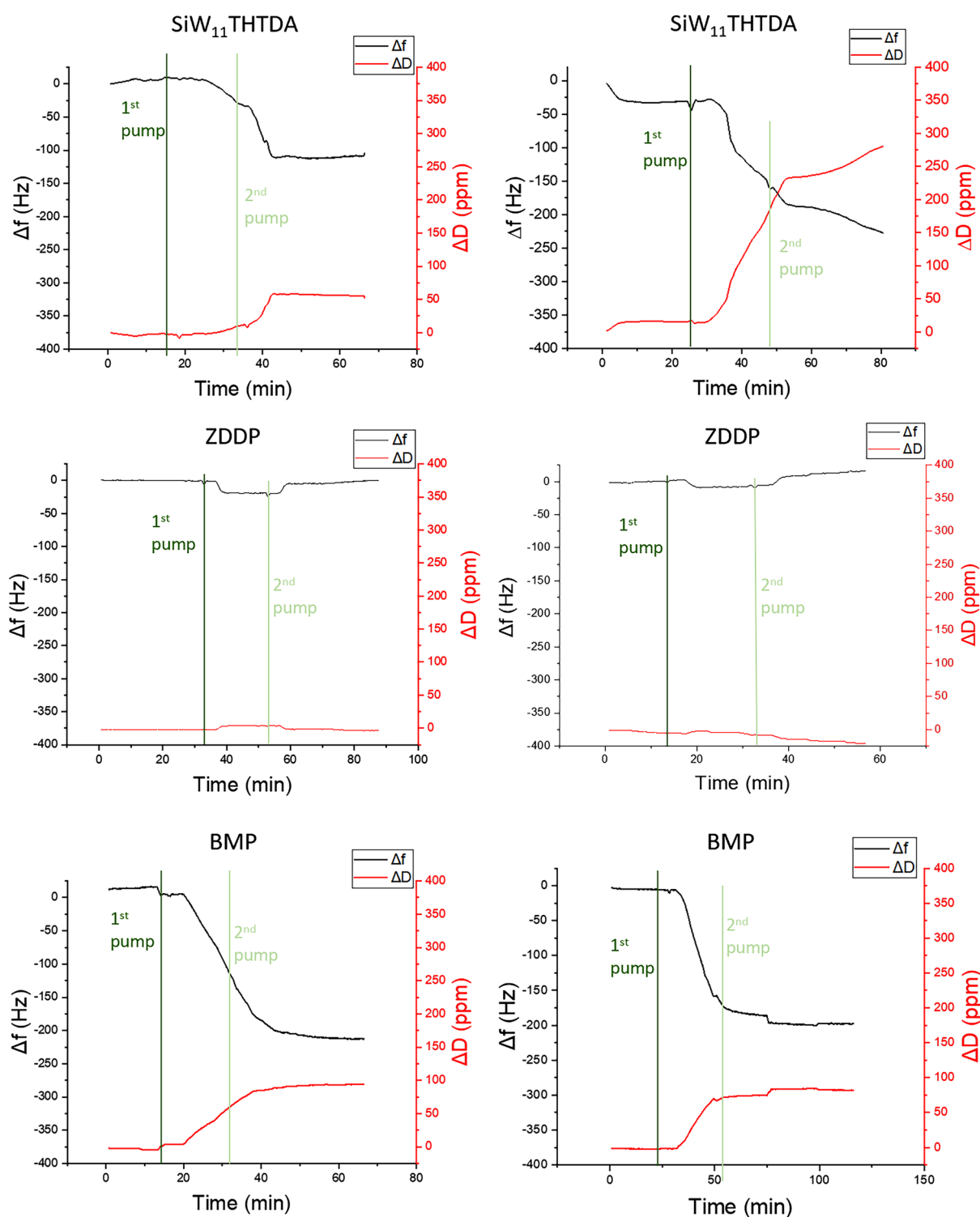


Fig. 6 Adsorption data (frequency change, Δf , and dissipation change, ΔD) for all tested blends in the different substrates. Two vertical lines indicate when the first (adding the additive, darker green)

and second pump (rinsing with plain PAO8, lighter green) took place. Part of this dataset has been previously reported in another publication [14]

to increased interfacial shear, whereas the softer IL-based adsorbed layers would likely result in lower friction. Surprisingly, this does not align with the frictional behaviour observed in this work, where similar friction is found for all additives with one exception (Fig. 2). On 52,100, BMP showed similarly low friction to ZDDP up to the point of 80 m sliding, where the friction rose for BMP, potentially due to a tribofilm formation and increased roughness. Before this shift, the lower friction could be attributed to the favourable properties of the strongly adsorbed film. SiW₁₁THTDA, however, behaved more like the base lubricant, exhibiting higher friction than BMP and ZDDP, suggesting that the properties of its adsorbed layer on this substrate were less effective in reducing friction.

On 316L, all additives decreased friction effectively, with the main difference being on the extent of the running-in period. The similar friction-reducing behaviour across additives, despite opposing adsorption behaviour, suggests that at room temperature, static adsorption measurements do not fully explain the tribological behaviour, and that other factors, such as tribochemical reactions, play a significant role in dictating friction performance at the testing conditions chosen for this work. Indeed, the presence of Zn, P, and S atoms inside the wear tracks was found for ZDDP (Table 4) is a clear indication of a tribochemical process taking place in addition to adsorption, as it will be further explained later. This tribochemical process results in a S, P, and/or Zn tribofilm formation that prevents direct contact of the solid surfaces thus effectively reducing wear [5, 27, 28]. Given the consistency showed by ZDDP, it cannot be neglected that its performance may be influenced, and perhaps even mediated, by its adsorption behaviour. This is however not the case for the IL-based additives, for which their strong adsorption on both substrates does not result in paralleled tribochemical reactions on 316L and 52,100 (Table 4). Albeit the experimental limitations, adsorption likely contributes to the observed friction reduction after the running-in, especially in the cases of BMP and SiW₁₁THTDA, where the viscoelasticity of the adsorbed layer could promote friction reduction. Unfortunately, further analysis on the adsorbed layer properties cannot be performed due to the viscosity of the base lubricant exceeding the capabilities of the QCM device. It is however possible that the strong adsorption, especially present in the case of the emulsion-forming blends, is a partial consequence of the additives wetting on the sensor surface irreversibly, where plain PAO8 would not be able to remove them effectively. This is, however, unlikely to be the sole reason behind substrate affinity of the additives, especially for SiW₁₁THTDA, since, as observed in Fig. 8, additives are found for the different substrates, suggesting substrate specificity beyond simple physical wetting of the surface.

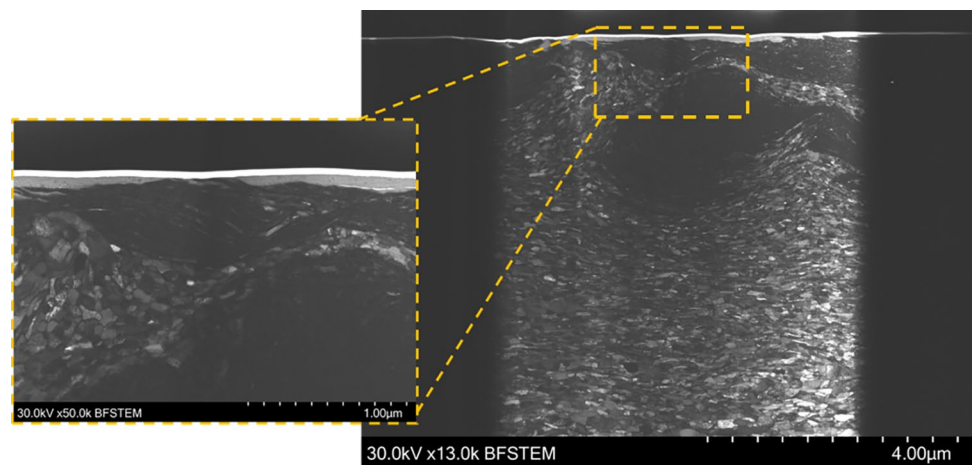
For IL-based additives, the research on their mechanisms of action is still under development, and thus, they are less well understood than in the case of ZDDP. Two primary proposals exist: the formation of an adsorbed layer and the development of a protective tribofilm [29]. However, identifying the exact mechanisms remains challenging due to the intrinsic variability in structural characteristics within this broad family of compounds. Nonetheless, one key takeaway from our findings is that efficient contact with the substrate alone does not guarantee effective interaction of ILs with the substrate, nor does it ensure efficient friction and wear reduction. Our results suggest that the adsorbed layer mechanism observed in some IL-based additives, involving IL anions followed by cations [30], may not be predominant for the additives in this study. Instead, tribochemical interactions may be necessary to achieve the observed friction-reducing and anti-wear effects. The findings in this work suggest a possible two-phase mechanism, where initial adsorption is necessary for a subsequent tribochemical reaction. This is supported by the comparison of the adsorption results for the two metal alloys tested in this work.

4.2 Effect of Metal Alloy Chemistry on Friction and Wear

The friction evolution trends observed in Fig. 2 show that 316L goes through a running-in period prior to friction stabilization, whereas 52,100 enters the friction steady state quickly. The inherent strength and wear resistance of 52,100 play a crucial role in this behaviour. Once the steady state is achieved, the differences in friction between additives is smaller for 316L than for 52,100. For 52,100, a minimal change in friction was observed between plain PAO8 and PAO8 with additives during the 100 m tests. The wear rate results on 52,100 indicate that only ZDDP significantly improves wear. This observation suggests different interaction mechanisms between ZDDP, BMP, and SiW₁₁THTDA with 52,100. On the other hand, 316L showed a consistent and significant effect of all additives in terms of both friction and wear rate with respect to plain PAO8. Plain PAO8 showed a long running-in period and higher friction values and wear rates. The additives substantially decreased the running-in period and lowered friction and wear rate to values comparable to those seen with 52,100. This clearly indicates that the additives perform differently depending on the chemistry and mechanical properties of the metal alloy used.

The cross-sectional images in Fig. 5 reveal different effects of ZDDP compared to BMP and SiW₁₁THTDA on the subsurface metal microstructure. However, all three additives exhibit successful anti-wear behaviour and friction on 316L with a similar wear track morphology (Fig. 4). Plain PAO8 on 316L showed the highest CoF and wear across all tests, where a large recrystallization area with significant

Fig. 7 Scanning (transmission) electron microscope image of 316L sample lubricated with $\text{SiW}_{11}\text{THTDA}$ in PAO8



grain refinement is observed. BMP and $\text{SiW}_{11}\text{THTDA}$ also experienced high degree of recrystallization in 316L, despite having lower CoF and wear values. However, they differ on the running-in period, indicating that the initial high friction during the running-in period plays an important role on subsurface deformation. Indeed, in a Scanning Transmission Electron Microscopy (STEM) analysis of the wear track of $\text{SiW}_{11}\text{THTDA}$ in 316L (Fig. 7), an extensive area of nanometric grain refinement is observed. This could be either due to increased shear forces or the role of the adsorbed layer. If the latter is true, this suggests that $\text{SiW}_{11}\text{THTDA}$ has a stronger chemical affinity with the metal than the other additives potentially inducing more shear induced recrystallization, while maintaining low and stable CoF after the running-in. On the other hand, BMP and ZDDP present a much smaller grain refinement area than $\text{SiW}_{11}\text{THTDA}$, being greater for BMP than for ZDDP.

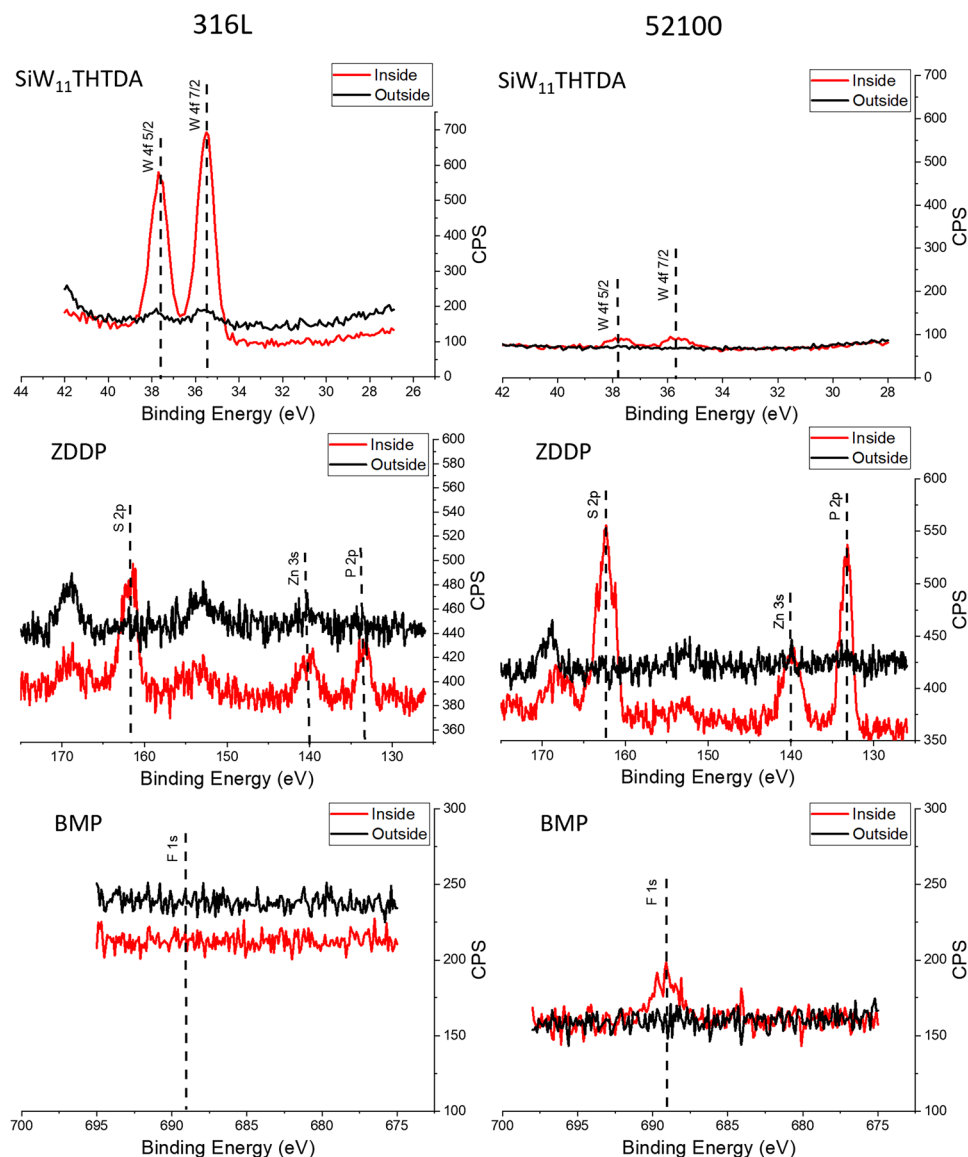
For 52,100, differences in CoF among additives arise, while all having negligible running-in. Thus, a similar relationship between CoF and subsurface plastic deformation appears for 52,100, where BMP and $\text{SiW}_{11}\text{THTDA}$ show more pronounced plastic deformation and higher CoF, evident through elongated grains near the surface (Fig. 5). ZDDP produced minimal deformation and the lowest CoF and wear. Nonetheless, given the inherent strength of 52,100, friction-induced subsurface microstructural changes were relatively superficial for all additives, where rapid transition to the bulk microstructure can be observed in the FIB cross-sectional images.

As mentioned earlier, chemistry seems to play a much relevant role in friction and wear evolution on 316L. The high-resolution XPS scans in Fig. 8 provide further insight into the superficial interactions of each additive, beyond the survey analysis. A discrepancy with the survey analysis scan arises from the increased sensitivity of the high-resolution scans, which can detect smaller amounts of elements compared to the broader, less detailed survey scan used for the

quantification in Table 4. The high-resolution scans (Fig. 8) for $\text{SiW}_{11}\text{THTDA}$ demonstrated substantial differences across substrates, i.e. while a strong signal for W was found on 316L, indicative of tribofilm formation, no comparable signal was found for 52,100. This lack of W on 52,100 suggests that the effectiveness of $\text{SiW}_{11}\text{THTDA}$ in reducing friction and wear strongly depends on tribofilm formation (i.e. tribochemical reactions), reinforcing the correlation between substrate-additive chemical interactions and friction reduction and anti-wear properties. For ZDDP, signals of P 2p (133 eV), S 2p (162 eV), and Zn 3s (140 eV) were found on both substrates, indicating effective tribofilm formation, which supports the observed reduction in friction and wear. Quantification from the survey scan indicated higher atomic percentages of these elements for 52,100 than for 316L (Table 4). This suggests that decomposition products of ZDDP, containing P, S, and Zn, occurred easier on 52,100 than on 316L. No F or P was detected in for BMP on 316L, both inside and outside the wear track. However, a small F 1s (689 eV) signal was observed in 52,100 inside the wear track. This could be an indication of the onset of a thicker tribofilm formation on 52,100 for BMP.

These contrasting behaviours imply that the mechanisms behind the anti-wear properties of the additives are controlled by the chemistry of the substrate. Since the main differences between these two substrates stem from their chemical composition and microstructure, it is essential to study if these influence the metal-additive interaction, especially for the POM-IL. The chemical composition and microstructure of both substrates are found in Fig. 1 and Table 2, where the most significant differences stem from the higher content of Cr, Ni, and Mo in 316L. In addition, while Cr is found in its metallic form in 316L, it is found in the form of chromium-rich iron carbide precipitates in 52100 [31]. To further study the effect of these compounds in the POM-IL lubricated sample, an in-depth XPS analysis of 316L lubricated with $\text{SiW}_{11}\text{THTDA}$ in PAO8 was carried

Fig. 8 High-resolution XPS spectra of the metal substrates inside and outside the wear track for all additives at 1 wt.% in PAO8. Part of this dataset has been previously reported in another publication [14]

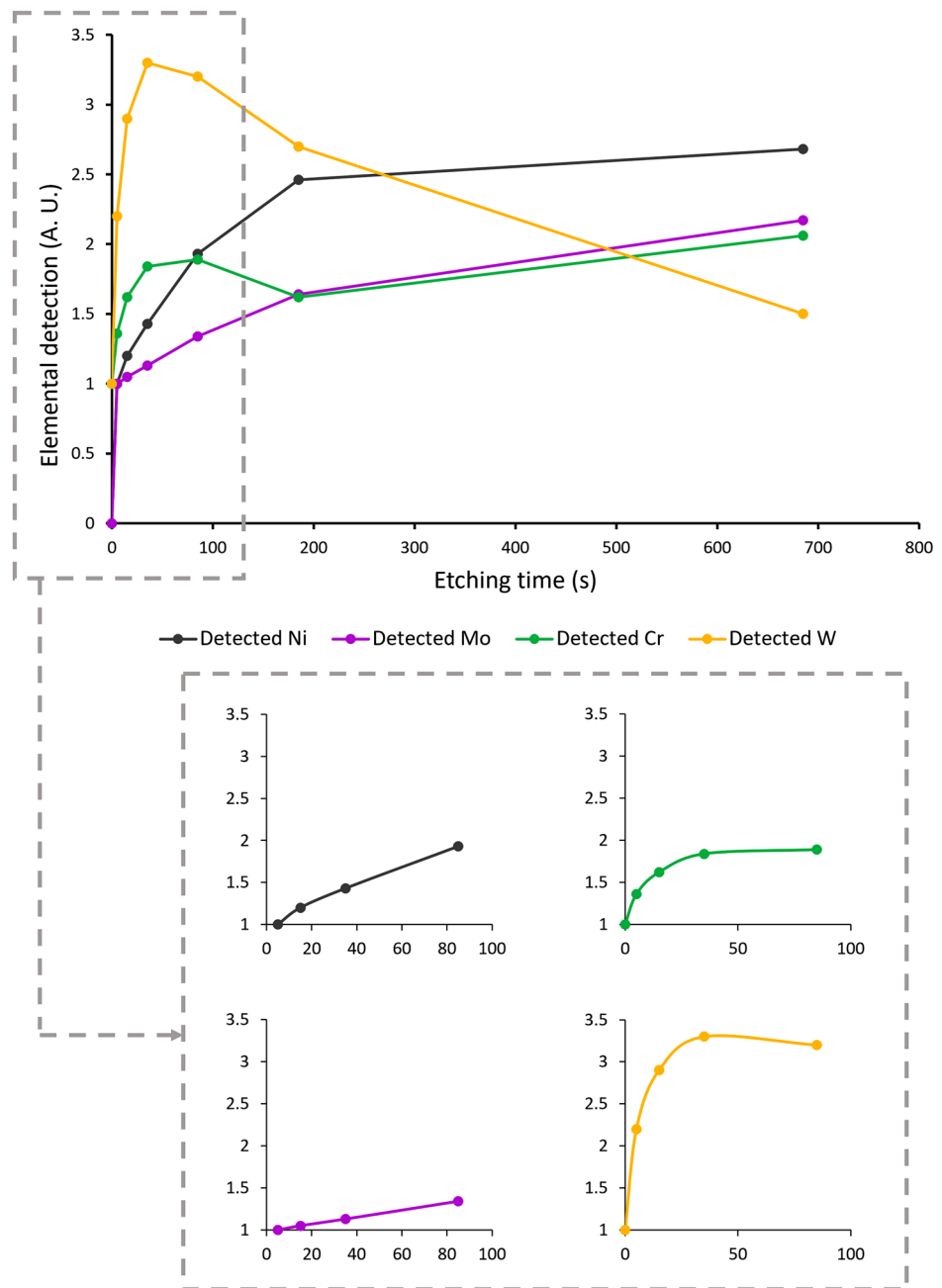


out, with measurements inside and outside the wear track. The depth evolution of key elements (Ni, Cr, Mo, and W) was determined through an etching process, acquiring measurements from 0 to 685 s (Fig. 9). The full evolution as well as comparison with outside the wear track is found in Figure S5 and Figure S6 in the supplementary material.

Ni and Mo present a similar steep evolution with depth, differing from Cr and W. Two different oxidation states for Cr were detected (Fig. S7), Cr(III) oxide and/or hydroxide (in the form of a protective film on the surface of 316L, i.e. the so-called passive film) at the beginning of the etching process, and Cr⁰ from the bulk of the material as time progresses. The Cr(III) present in the outer layer of 316L replenishes as the tribotest advances due to its reaction with atmospheric oxygen (the so-called repassivation process). It is interesting to notice the correlation between Cr(III) and

W evolution (especially clear in the zoomed in graphs), suggesting a strong metal substrate–POM interaction. Indeed, it makes chemical sense that a metal Cr in its cationic form (Cr(III)) is reactive with the POM anion, since the chemical nature of both species is clear opposites. The POM anion is a Lewis base, given its high electron donor character, and Cr in Cr₂O₃ presents characteristics of a Lewis acid. The theory dictates that a Lewis acid has affinity and will react with a Lewis base in a Lewis acid–base reaction. This reaction suggests a significant interaction between the POM-IL and 316L potentially yielding a Cr–W bond, strengthening the material (as indicated by the thick recrystallized layer in Fig. 7). Indeed, in a work by Tomsa et al. [32], interactions between a Cr(III) cation and a W-containing lacunary POM driven by coordination chemistry have been described.

Fig. 9 Elemental depth evolution of Ni, Cr, Mo, and W inside the wear of the 316L sample lubricated with SiW₁₁THTDA in PAO8. 100 s etching area is represented separately for each individual element. In the zoomed graphs, the contribution from Cr⁰ has been removed and only Cr(III) is plotted



This evidence gives a good basis in explaining why 316L samples lubricated with SiW₁₁THTDA perform better than those of 52,100. The presence of Cr(III) seems to be optimal for an anchorage of the W-containing POM species, which is able to then react, or bind to the Cr(III)-rich layer and provide protection in terms of reduced friction and wear.

4.3 Influence of Steric Factors and Work-Hardening on Additive Performance

Although similar trends between BMP and SiW₁₁THTDA have been observed, they have a significantly different

chemical nature. While BMP has a 1:1 anion-to-cation ratio, the POM-IL has a 1:8 ratio due to the large negative charge of the POM anion. This could significantly influence the affinity with the metal substrate as well as its steric accessibility to the surface, as illustrated in Fig. 10, leading to potential variations in their tribochemical activity. Additionally, the triboactive atoms in each structure also differ: BMP contains P and F, while W is the primary triboactive element for SiW₁₁THTDA. Indeed, the surface chemical analysis detected only a minor F signal inside the wear track of 52,100 for BMP, which, along with previous findings [33], suggests that BMP is mostly inducing the formation of an

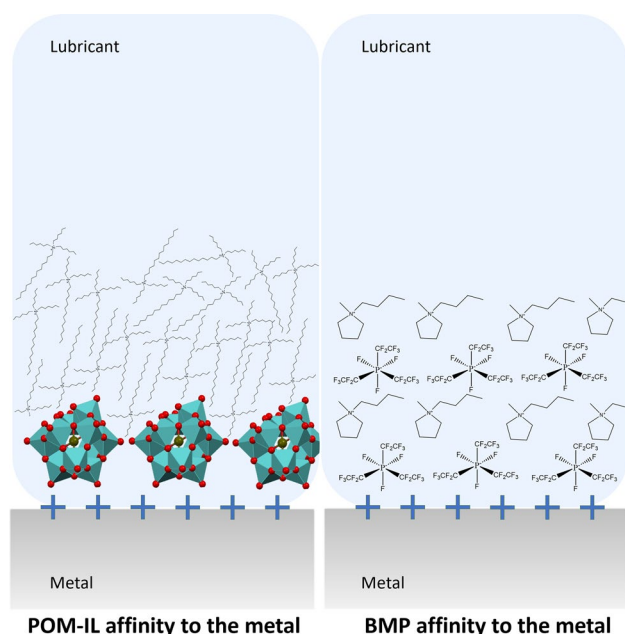


Fig. 10 Proposed affinity differences between $\text{SiW}_{11}\text{THTDA}$ and BMP onto a metallic substrate

oxide-rich tribofilm on both metal substrates, and additionally forming FeF_3 on 52,100 only. Despite that, the tribofilm generated by BMP provided with significant friction and wear reduction on 316L, but negligible benefits on 52,100. Furthermore, $\text{SiW}_{11}\text{THTDA}$ was most efficient on 316L than on 52,100, clearly indicating that both IL undergo different mechanisms depending on the type of metal used as substrate. Interestingly, ZDDP was equally efficient in both substrates.

In the case of 316L, the IL-based additives seem to be promoting a work-hardening effect (understood as the difference in hardness between inside and outside the wear track), as can be observed in Table 5. The largest work-hardening is obtained with $\text{SiW}_{11}\text{THTDA}$, followed by BMP. This agrees with the observed plastic deformation area for these two ILs, as illustrated in Fig. 5, and the improved anti-wear properties on 316L, being largest for $\text{SiW}_{11}\text{THTDA}$. The absence of triboactive elements (P and F) inside the wear track suggests that BMP's performance is mostly driven by mechanical effects rather than direct tribochemical interactions. However, W is found in the wear scar of 316L, suggesting that this substrate is prone to interact especially with the W atom of $\text{SiW}_{11}\text{THTDA}$. This highlights the importance of identifying improved mechanical properties of the substrate's surface, rather than solely detecting the presence of active elements when assessing tribological performance. The case of ZDDP presents a different scenario, where its work-hardening is comparable to that of plain PAO8, suggesting

Table 5 Hardness measurements of 316L and 52,100 discs after testing with the different lubricant blends

Lubricant for tribotest	Vickers hardness	
	316L	52,100
Untested metal alloy	267.9 ± 13.3	193.3 ± 4.5
Plain PAO8	387.9 ± 8.1	285.3 ± 9.1
ZDDP in PAO8	385.2 ± 3.3	234.3 ± 5.0
BMP in PAO8	401.3 ± 15.6	273.6 ± 5.1
$\text{SiW}_{11}\text{THTDA}$ in PAO8	451.7 ± 26.4	240.3 ± 1.5

While all the discs tested with lubricant blends were evaluated for hardness inside the wear track, the measurement for the substrates was carried out on an untested, polished sample

that the mechanism behind the anti-wear performance likely differs between the additives.

The work-hardening effect on 52,100 was considerably less pronounced, which is in accordance with the smaller recrystallization area observed in Fig. 5. This effect can be attributed to the microstructure of this substrate, where carbide precipitates restrict large-scale plastic deformation and consequently hinder the hardening of the surface. Indeed, this is confirmed by the hardness values obtained inside the wear track for all additives, which did not show any evidence of inducing any additional hardening on the substrate that could contribute to the anti-wear behaviour. Among the tested additives, only ZDDP effectively reduced wear on 52,100, suggesting that its performance is primarily governed by tribochemical interactions rather than by work-hardening. The lack of $\text{SiW}_{11}\text{THTDA}$ constituent atoms detected on the 52,100 wear track suggests that it does not form an effective tribofilm on this substrate. This, together with the lack of work-hardening effect, justifies the lack of improved friction-reducing or anti-wear properties on this substrate and highlights the differences between the additives' performance.

5 Conclusions

An in-depth analysis of polyoxometalate-ionic liquids as lubricant additives on different metallic substrates has revealed key differences from other additives, such as ZDDP, a common anti-wear additive, and a more traditional IL structures. Based on the experimental findings from this work, the following conclusions can be drawn:

- Adsorption behaviour varies significantly among additives. While ZDDP exhibited physisorption, the IL additives underwent chemisorption, being a trend that remained consistent across both substrates.

- ZDDP's tribological performance is substrate-independent. Its anti-wear and friction-reducing behaviour, as well as the presence of active chemical elements in the tribofilm, show minimal variation between substrates with a minimal effect on work-hardening.
- Ionic liquids show substrate-dependent tribological behaviour. Despite consistent chemisorption, their anti-wear and friction-reducing effects differ according to the chemical composition of the substrates. This suggests that adsorption alone does not fully account for performance, and thus a combined mechanism, involving strong adsorption followed by tribochemical reactions, is crucial for their anti-wear and friction-reducing properties.
- The effectiveness of the POM-IL depends on both the chemical composition and microstructure of the substrate. Specifically, the interaction of W atoms with Cr(III) metal cations appears to be a key factor in the POM-IL's ability to reduce wear and friction. Thus, the availability of Chromium ions in the metal substrate is crucial for activating the tribochemical reactions that lead to tribofilm formation and/or work-hardening.
- Work-hardening contributes to anti-wear performance in 316L. SiW₁₁THTDA leads to a significant work-hardening in 316L, followed by BMP and ZDDP, potentially explaining its superior anti-wear behaviour beyond only chemical interactions.
- The absence of tribofilm formation and work-hardening renders the POM-IL ineffective, as seen for 52,100. Despite strong adsorption of SiW₁₁THTDA on 52,100, the lack of tribofilm formation and/or significant work-hardening resulted in no observable anti-wear or friction-reducing behaviour.

Supplementary Information The online version contains supplementary material available at <https://doi.org/10.1007/s11249-025-02033-9>.

Acknowledgements The authors would like to acknowledge financial support from the Norwegian Infrastructure for Micro- and Nanofabrication (NORFAB, project 295864), the enabling technologies at NTNU (project 81771596), and the Infrastructure for Materials Research for Transporting Hydrogen (SMART-H, project 296197). This work was also funded through the grant PID2022-141276OB-I00 and CEX2023-001286-S funded by MCIN/AEI/<https://doi.org/10.13039/501100011033> (Ministerio de Ciencia e Innovación/Agencia Estatal de Investigación, Spain). This study was supported by MCIN with funding from the European Union NextGenerationEU (PRTR-C17.I1) promoted by the Government of Aragón. Authors acknowledge the use of instrumentation as well as the technical advice provided by the National Facility ELECMi ICTS, node Laboratorio de Microscopias Avanzadas (LMA) at Universidad de Zaragoza.

Author Contributions M. L. Casasin-Garcia has contributed with the experimental work, drafting the first version of the manuscript, and the analysis and discussion of the results. S.G. Mitchell has contributed with synthesis of the POM-IL, writing parts of the manuscript and the

analysis and discussion of the results. N. Espallargas conceived the project, secured funding for it, has supervised the experimental work of M.L. Casasin-Garcia, has written parts of the manuscript, and has contributed to the analysis and discussion of the results. All authors contributed to the proposal of tables and figures.

Funding Open access funding provided by NTNU Norwegian University of Science and Technology (incl St. Olavs Hospital - Trondheim University Hospital).

Data Availability No datasets were generated or analysed during the current study.

Declarations

Conflict of interest The authors declare no competing interests.

Open Access This article is licensed under a Creative Commons Attribution 4.0 International License, which permits use, sharing, adaptation, distribution and reproduction in any medium or format, as long as you give appropriate credit to the original author(s) and the source, provide a link to the Creative Commons licence, and indicate if changes were made. The images or other third party material in this article are included in the article's Creative Commons licence, unless indicated otherwise in a credit line to the material. If material is not included in the article's Creative Commons licence and your intended use is not permitted by statutory regulation or exceeds the permitted use, you will need to obtain permission directly from the copyright holder. To view a copy of this licence, visit <http://creativecommons.org/licenses/by/4.0/>.

References

1. Agency, U. S. E. P. *Environmentally Acceptable Lubricants*. https://www3.epa.gov/nepdes/pubs/vgp_environmentally_acceptable_lubricants.pdf (2011) https://doi.org/10.1007/978-3-642-22647-2_100214.
2. Ngo, D., He, X., Luo, H., Qu, J., Kim, S.H.: Competitive adsorption of ionic liquids versus friction modifier and anti-wear additive at solid/lubricant interface—speciation with vibrational sum frequency generation spectroscopy. *Lubricants* **8**, 1–18 (2020)
3. Guegan, J., Southby, M., Spikes, H.: Friction modifier additives, synergies and antagonisms. *Tribol. Lett.* **67**, 1–12 (2019)
4. Marinescu, I.D., Rowe, W.B., Dimitrov, B., Ohmori, H.: Process fluids for abrasive machining. *Tribol. Abras. Mach. Processes* (2013). <https://doi.org/10.1016/b978-1-4377-3467-6.00015-x>
5. Spikes, H.: The history and mechanisms of ZDDP. *Tribol. Lett.* **17**, 469–489 (2004)
6. Rensselaar, J. Van. Lubrication and tribology trends and challenges in electric vehicles. https://www.stle.org/files/TLTArchives/2020/07_July/Webinars.aspx?WebsiteKey=a70334df-8659-42fd-a3bd-be406b5b83e5#.Xx_cfx-cpiM.linkedin (2020).
7. Afton Chemicals. Engine oils componentry – zinc dialkyl dithiophosphate (ZDDP). <https://www.aftonchemical.com/Afton/media/Documents/Product-Stewardship-Summaries-ENGINE-OILS-COMPONENTRY-ZDDP.pdf>.
8. Ye, C., Liu, W., Chen, Y., Yu, L.: Room-temperature ionic liquids: a novel versatile lubricant. *Chem. Commun.* **21**, 2244–2245 (2001)
9. Cai, M., Yu, Q., Liu, W., Zhou, F.: Ionic liquid lubricants: when chemistry meets tribology. *Chem. Soc. Rev.* **49**, 7753–7818 (2020)

10. Liu, W., Ye, C., Gong, Q., Wang, H., Wang, P.: Tribological performance of room-temperature ionic liquids as lubricant. *Tribol. Lett.* (2002). <https://doi.org/10.1023/A:1020148514877>
11. Aureliano, M.: 1, 2. The future is bright for polyoxometalates. *BioChem* **2**, 8–26 (2022)
12. Cisson, C.M., Rausina, G.A., Stonebraker, P.M.: Human health and environmental hazard characterisation of lubricating oil additives. *Lubr. Sci.* **8**, 145–177 (1996)
13. Rokosz, M.J., et al.: Characterization of phosphorus-poisoned automotive exhaust catalysts. *Appl. Catal. B Environ.* **33**, 205–215 (2001)
14. Casasin-Garcia, M.L., Khanmohammadi, H., Mitchell, S.G., Espallargas, N.: Polyoxometalate-ionic liquids (POM-ILs) — a new type of ionic liquid additive family for lubricants. *RSC Adv.* **15**, 1275–1289 (2025)
15. Misra, A., et al.: Polyoxometalate-ionic liquids (POM-ILs) as anticorrosion and antibacterial coatings for natural stones. *Angew. Chemie Int. Ed.* **57**, 14926–14931 (2018)
16. Rajkowska, K., et al.: Antifungal activity of polyoxometalate-ionic liquids on historical brick. *Molecules* (2020). <https://doi.org/10.3390/molecules25235663>
17. Zhang, X., Xiao, Y., Cai, Y.: Effect of Ni element on microstructure and properties of cold-rolled 316 L austenitic stainless steel. *Mater. Res. Express* **11**, 036521 (2024)
18. Bjerregaard, L., Geels, K., Ottesen, B. & Rückert, M. *Metalog guide. Your Guide to the Perfect Metallographic Structure. Ref_Prep_Sample* (Struers A/S, 2020).
19. Hamrock, B.J., Dowson, D.: Ball Bearing Lubrication (The Elastohydrodynamics of Elliptical Contacts). *J. Lubr. Technol.* **104**, 279–281 (1982)
20. Archard, J.F.: Contact and rubbing of flat surfaces. *J. Appl. Phys.* (1953). <https://doi.org/10.1063/1.1721448>
21. Bruce, R.W.: Handbook of lubrication and tribology. Volume II: Theory and design, p. 15. CRC Press, Boca Raton (2012)
22. NIST. NIST X-ray Photoelectron Spectroscopy Database (SRD 20), Version 5.0. <https://srdata.nist.gov/xps/ElmComposition>.
23. Huang, G., Yu, Q., Ma, Z., Cai, M., Liu, W.: Probing the lubricating mechanism of oil-soluble ionic liquids additives. *Tribol. Int.* **107**, 152–162 (2017)
24. Fedorov, M.V., Kornyshev, A.A.: Ionic liquids at electrified interfaces. *Chem. Rev.* **114**, 2978–3036 (2014)
25. Sauerbrey, G.: Verwendung von Schwingquarzen zur Wägung dünner Schichten und zur Mikrowägung. *Physik* (1959). <https://doi.org/10.1007/BF01337937>
26. Dixon, M.C.: Quartz crystal microbalance with dissipation monitoring: Enabling real-time characterization of biological materials and their interactions. *J. Biomol. Tech.* **19**, 151–158 (2008)
27. Ashford, J.S., Bretherick, L., Gould, P.: The thermal decomposition of zinc di-(4-methylpentyl-2) dithiophosphate. *J. Appl. Chem.* **15**(4), 170–178 (1965)
28. Taylor, L., Dratva, A., Spikes, H.A.: Friction and wear behavior of zinc dialkyl dithiophosphate additive. *Tribol. Trans.* **43**, 469–479 (2000)
29. Xiao, H.: Ionic liquid lubricants : basics and applications. *Tribol. Trans.* **60**, 20–30 (2017)
30. Xie, G., Luo, J., Guo, D., Liu, S.: Nanoconfined ionic liquids under electric fields. *Appl. Phys. Lett.* (2010). <https://doi.org/10.1063/13292213>
31. Wijnarko, W. *Ionic Liquids as Additives in Low Viscosity Lubricants – A Surface Adsorption and Tribofilm Study*. (Norwegian University of Science and Technology, 2022).
32. Tomşa, A.R., et al.: Synthesis, spectroscopic and electrochemical characterization of a new chromium (III) substituted dawson polyoxometalate. *Stud. Univ. Babes-Bolyai Chem.* **4**, 95–105 (2009)
33. Wijnarko, W., Khanmohammadi, H., Espallargas, N.: Effect of steel hardness and composition on the boundary lubricating behavior of low-viscosity PAO formulated with dodecanoic acid and ionic liquid additives. *Langmuir* (2022). <https://doi.org/10.1021/acs.langmuir.1c02848>

Publisher's Note Springer Nature remains neutral with regard to jurisdictional claims in published maps and institutional affiliations.